Research Square

Preprints are preliminary reports that have not undergone peer review.
They should not be considered conclusive, used to inform clinical practice,
or referenced by the media as validated information.

Clinicopathological Determinants of Prognosis in Hepatocellular Carcinoma: Integrating Histopathology with an IHC-Based Molecular Subclassification

Sophie von Sachsen-Coburg
University of Regensburg
Katja Evert
University of Regensburg
Elena Preis
University of Regensburg
Marion Vogl
University of Regensburg
Philipp Kreiner
University Hospital Regensburg
Paul Kupke
University Hospital Regensburg
Jens Werner
University Hospital Regensburg
Bettina Lambert
University of Regensburg
Monika Kerscher
University of Regensburg
Tabea Globuschütz
University Hospital Regensburg
Philipp Heumann
University Hospital Regensburg
Arne Kandulski
University Hospital Regensburg
Monika Klinkhammer-Schalke
University of Regensburg
Diego F. Calvisi
University of Regensburg
Matthias Evert
University of Regensburg

Kirsten Utpatel
University of Regensburg
Alexander Scheiter
alexander.scheiter@med.uni-regensburg.de

University of Regensburg

Research Article

Keywords:

Posted Date: September 14th, 2026

DOI: https://doi.org/10.21203/rs.3.rs-10490174/v1

License: This work is licensed under a Creative Commons Attribution 4.0 International License.
Read Full License

Additional Declarations: Competing interest reported. The authors declare the following competing interests: KU: received honoraria from Roche, BMS, Lilly, AMGEN, Minarini Stemline.

Abstract

Background

Hepatocellular carcinoma (HCC) is a biologically heterogeneous malignancy that has undergone major therapeutic changes over the last two decades. Here, a real-world clinicopathological cohort integrating morphology, prognostic parameters, immunohistochemical surrogate markers for molecular stratification, and treatment outcome data is presented.

Methods

We performed a retrospective single-center study of 597 patients with histologically confirmed HCC (or occasional cases of combined hepatocellular-cholangiocarcinoma) diagnosed at the Institute of Pathology, University of Regensburg, between 2000 and 2024. Clinical, pathological, laboratory, and follow-up data were merged with regional cancer registry data. Survival analyses were performed using Kaplan-Meier estimates and univariate and multivariate Cox proportional hazards regression. In a tissue microarray-based subcohort, immunohistochemistry for p53, Cyclin A2, Cyclin E1, β-catenin, and L-FABP1 was evaluated as a surrogate for a recently proposed molecular subclassification. Systemic treatment response and progression-free survival were assessed in patients with available follow-up data.

Results

The cohort comprised 486 men and 111 women, with a median age at diagnosis of 70 years in men and 67 years in women. Cirrhosis (49.7%), viral hepatitis (24.0%), diabetes mellitus (33.8%), arterial hypertension (45.2%), and steatosis hepatis (24.3%) were frequent background conditions. Median overall survival was 52 months. Survival declined with increasing grade and with incomplete resection. In multivariate Cox regression, older age, advanced T category, vascular invasion, positive resection margins, poor differentiation, macrotrabecular-massive (MTM) subtype, absence of tumor capsule, steatosis, and elevated alkaline phosphatase showed prognostic relevance, with age, T category, vascular invasion, resection status, MTM subtype, tumor capsule, and alkaline phosphatase emerging as particularly robust predictors. In the tissue microarray cohort, p53-high expression was independently associated with worse overall survival, whereas combined Cyclin A2/E1 high expression was significant in univariate analysis. L-FABP1 loss and nuclear β-catenin accumulation were not associated with outcome. Patients treated with atezolizumab/bevacizumab showed higher response rates than those treated with sorafenib.

Conclusions

This quarter-century single-center study highlights the multifactorial background, morphological diversity, and prognostic heterogeneity of HCC in routine clinical practice. Established clinicopathological variables remain the strongest determinants of survival, while p53 immunohistochemistry may provide additional prognostic information as an accessible molecular surrogate. The data further reflect the changing systemic treatment landscape from sorafenib to immunotherapy-based regimens in a real-world cohort.

Background

Hepatocellular carcinoma (HCC) is the most common primary malignant tumor of the liver, arising from hepatocytes and accounting for approximately 90% of primary liver cancers [1]. It represents a major global health burden and remains one of the leading causes of cancer-related mortality worldwide [2]. Incidence rates show a marked sex disparity, with men affected two- to threefold more frequently than women [3].

HCC typically develops in the context of chronic liver disease, most commonly in the presence of liver cirrhosis, which remains one of the most important risk factors regardless of the underlying etiology [4]. Major exogenous risk factors include viral hepatitis B and C (HBV/HCV), as well as excessive alcohol and tobacco consumption. Increasing attention is also being paid to metabolic syndrome [5]. Conditions such as type 2 diabetes mellitus, obesity, arterial hypertension, and dyslipidemia represent metabolic risk factors that can promote the development of metabolic dysfunction–associated steatotic liver disease (MASLD) and metabolic dysfunction–associated steatohepatitis (MASH). In Western countries, MASH-related HCC accounts for approximately one-fifth of cases and is increasingly recognized as a major underlying cause of HCC [6].

Histologically, HCC can be classified according to the World Health Organization (WHO) Classification of Tumours of the Digestive System (6th edition, 2026) into several subtypes [7]. The majority of cases are categorized as conventional HCC (“not otherwise specified”, NOS-HCC). In addition, eight further subtypes have been described, listed here in decreasing order of frequency: steatohepatitic HCC (SH-HCC), clear cell HCC, macrotrabecular-massive HCC (MTM-HCC), which is associated with poor prognosis, elevated serum alpha-fetoprotein (AFP) levels, and TP53 mutations; scirrhous HCC; chromophobe HCC; fibrolamellar carcinoma (FLC), which predominantly occurs in younger patients without cirrhosis, and the two rare inflammatory subtypes, neutrophil-rich and lymphocyte-rich HCC [8, 9].

Beyond histological classification, HCC can also be stratified on a molecular level, which is becoming increasingly important in the context of personalized therapy and research. Although immunohistochemical markers currently have limited direct impact on therapeutic decision-making, they may well serve as prognostic parameters. Approximately 25% of HCC tumors harbor therapeutically relevant mutations, most commonly involving the TERT promoter, TP53, and CTNNB1 [10]. Recently, Pan et al. [11] proposed an integrative molecular subclassification of HCC based on multiomic profiling of

529 tumors with validation in 807 external cases. This classification defines common subtypes driven by CTNNB1/APC, TP53, and AXIN1/IRF2 alterations, as well as rarer subgroups characterized by combined TP53 and CTNNB1 alterations, BAP1, CCNA2/CCNE1, or HNF1A inactivation. Importantly, several of these molecular subgroups can be approximated by immunohistochemical surrogate markers, including p53 overexpression, nuclear β-catenin accumulation, Cyclin A2/E1 overexpression, and L-FABP1 loss, providing a rationale for pathology-based substratification in routine formalin-fixed, paraffin-embedded (FFPE) cohorts, which we performed in this work.

The treatment of HCC has undergone substantial changes over the past two decades. Interdisciplinary treatment strategies and the integration of immunotherapy have significantly improved overall survival [12]. Prior to 2000, effective systemic treatment options were largely unavailable, as conventional chemotherapies demonstrated limited efficacy [10]. Based on the results of the phase III SHARP trial [13], the tyrosine kinase inhibitor (TKI) sorafenib was approved by the U.S. Food and Drug Administration (FDA) in November 2007, representing the first molecularly targeted therapy for advanced HCC [10, 14]. For many years, it remained the standard first-line treatment and significantly improved overall survival (OS) [14].

Since 2020, immunotherapy has moved to the forefront of HCC treatment. The results of the phase III IMbrave150 trial [15] demonstrated a breakthrough in the systemic treatment of advanced HCC through the combination of immune checkpoint inhibitors with anti-angiogenic agents [14, 16]. Consequently, the immune checkpoint inhibitor atezolizumab in combination with the monoclonal antibody bevacizumab (Atezo/Bev) received FDA approval in May 2020 and replaced sorafenib as the standard first-line therapy [10]. For patients who do not respond to or have contraindications to these newer combination therapies, further treatment options remain available, including sorafenib as well as lenvatinib, regorafenib, cabozantinib, and ramucirumab. Overall, current HCC management follows a multimodal approach, combining locoregional therapies (such as transarterial chemoembolization [TACE] or radioembolization) with systemic treatments to downstage tumors and enable surgical resection. An individualized therapeutic strategy is therefore essential to improve both treatment response and long-term outcomes in patients with HCC [10].

The aim of the present study is to analyze a local cohort from the region of Eastern Bavaria with regard to general risk factors, immunohistochemical and molecular subtypes, and therapeutic approaches.

Methods

Patient cohort

This retrospective study included all patients recorded at the Institute of Pathology, University of Regensburg, between 2000 and 2024. Patients were followed from the date of initial diagnosis until death or the last available follow-up. Data collection was conducted up to the predefined cut-off date of March 31, 2025.

Inclusion criteria comprised all patients with resected hepatocellular carcinoma (HCC) or combined hepatocellular–cholangiocellular carcinoma (cHCC-CCA) documented in the institutional pathology database during the study period, with corresponding records available in the clinical information system (SAP SE, Walldorf, Germany).

After data curation and integration with the regional cancer registry, a total of 597 patients were included, consisting of 486 men and 111 women. The cohort comprised 573 HCC cases and 24 cHCC-CCA cases.
All cases identified by the institutional pathology information system were independently reviewed by two board-certified pathologists with expertise in liver pathology to confirm the diagnosis according to the WHO Classification of Digestive System Tumours, 5th edition, before inclusion in the study.

Data acquisition and database construction

The institutional liver tumor registry was systematically reviewed and restricted to HCC and cHCC-CCA cases. These data were merged with cancer registry records to establish a comprehensive dataset. Patient identifiers were retrieved using the digital pathology system (dc-Pathos, NEXUS / Digital Pathology GmbH, Germany) based on histological specimen numbers.

Clinical data, including medical history, risk factors, laboratory values, imaging and staging reports, surgical records, and discharge summaries, were extracted from the hospital information system as well as data provided by the Regensburg Cancer Registry. Additional information was obtained from institutional archives where necessary. All data were compiled and structured in a database using Microsoft Excel, version 2019 (Microsoft Corporation, Redmond, WA, USA).

Due to long-term follow-up, multiple histological specimens were available for some patients. In total, 59 patients had two or more specimens obtained at different time points. For tumor staging, only the primary tumor was considered according to the TNM classification (8th edition, UICC/AJCC; 2018), ensuring that each patient was included only once in staging analyses.

Follow-up data were collected from clinical documentation of subsequent visits and staging examinations, where available. Laboratory parameters were obtained from routine clinical testing according to institutional standards.

Treatment response to systemic therapies was assessed, where possible, based on clinical reassessment and categorized as complete response (CR), partial response (PR), mixed response (MR), stable disease (SD), or progressive disease (PD). In some cases, response evaluation was not feasible due to incomplete documentation.

Statistical analysis

Statistical analyses were performed using GraphPad Prism, version 10.5.0 (GraphPad Software, San Diego, CA, USA).

Overall survival (OS) was defined as the time from diagnosis of the primary tumor to death or, in censored cases, the last follow-up or the cut-off date (March 31, 2025). Progression-free survival (PFS) was defined as the time from initiation of systemic therapy to the first documented progression or recurrence. Recurrence-free intervals were calculated from the time of tumor-free status to the occurrence of recurrence and classified according to residual tumor status (R0, R1, R2).
Overall survival (OS) and progression-free survival (PFS) were estimated using the Kaplan–Meier method, and differences between survival curves were assessed using the log-rank (Mantel–Cox) test. Median survival times are reported together with their corresponding 95% confidence intervals (95% CI). A p-value < 0.05 was considered statistically significant. Univariate and multivariate Cox proportional hazards regression models were used to evaluate associations between variables and survival outcomes, with results reported as hazard ratios (HRs), 95% confidence intervals (CIs), and p-values.

Continuous variables are presented as median with interquartile range (IQR) or mean ± standard deviation (SD), as appropriate, while categorical variables are reported as absolute numbers and percentages. Categorical variables, including treatment response and metastatic patterns, were expressed as numbers and percentages. Treatment sequences were visualized as a Sankey diagram using SankeyMATIC (https://sankeymatic.com).

Immunohistochemistry

Tissue microarrays (TMAs) were generated from 450 HCC cases with sufficient tumor material derived from liver resection specimens. In total, nine TMAs were constructed, each using cores with a diameter of 1.8 mm. In two patients, both the primary tumor and a subsequent resection specimen from recurrence were represented on the TMAs. Of note, the samples were treated as independent data points in downstream analyses. Retrospective evaluation confirmed that neither of the mentioned two cases belonged to any of the defined rare immunohistochemical subgroups, supporting their inclusion without introducing relevant bias. All remaining cases were represented once on the TMAs.

The TMAs were assessed for expression of the following immunohistochemical markers: TP53, Cyclin A2, Cyclin E1, β-catenin, and L-FABP1.

For automated immunohistochemistry, 2 µm sections were cut from the TMA blocks, deparaffinized, rehydrated, and processed on an automated staining platform (Ventana BenchMark ULTRA, Roche) in accordance with the manufacturer’s recommendations and the standard operating procedures of the Institute of Pathology, University of Regensburg. Signal detection was carried out using the OptiView DAB IHC Detection Kit to produce a 3,3'-diaminobenzidine (DAB) chromogenic reaction. Detailed information on primary antibodies, antigen retrieval conditions, dilutions, and supporting references is provided in Table S1.

Immunohistochemical staining was evaluated by a board-certified pathologist with experience in liver pathology, using the H-score for TP53, Cyclin A2, and Cyclin E1. Staining intensity was graded on a four-tier scale (0, 1+, 2+, 3+), corresponding to absent, weak, moderate, and strong staining, respectively. For

each case, the percentage of tumor cells exhibiting each intensity level was recorded and multiplied by the respective intensity score. The resulting values were summed to obtain a final H-score ranging from 0 to 300 [17].

L-FABP1 expression was specifically assessed for loss of staining, as this is considered a surrogate marker of underlying HNF1A mutations [18]. β-catenin immunoreactivity was evaluated with particular emphasis on nuclear localization, in contrast to physiological membranous staining, as nuclear accumulation is indicative of activating mutations in the corresponding gene [19].

For manual immunohistochemistry, 2 µm sections from formalin-fixed, paraffin-embedded (FFPE) tissue blocks were prepared. Sections were incubated at 70 °C for 30 minutes, followed by deparaffinization in xylene and rehydration through graded alcohols. Heat-induced antigen retrieval was performed for 8 minutes at 110 °C in citrate buffer (pH 6.0), followed by cooling in ice water. Endogenous peroxidase activity was blocked using Dako Peroxidase-Blocking Solution for 10 minutes. Primary antibodies were diluted in Dako Antibody Diluent and applied overnight at room temperature in a humidified chamber. After washing with Dako washing solution, sections were incubated with the secondary antibody ZytoChem Plus (HRP) Polymer anti rabbit/ anti mouse respectively for 60 minutes at room temperature. Following additional washing steps, chromogenic detection was performed using the Dako Liquid DAB+ Substrate Chromogen System. Counterstaining was carried out with Mayer's hemalum for 10 seconds.

Results

Baseline characterization of HCC cohort including survival parameters

A total of 597 histologically-confirmed patients with hepatocellular carcinoma (HCC) were included in this study cohort. The population was markedly male-dominated, comprising 486 men (81.4%) and 111 women (18.6%), consistent with the known epidemiology of HCC. The median age at diagnosis was slightly higher in men (70 years, IQR 63 – 77) compared to women (67 years, IQR 57 – 77). Age distribution across the cohort showed a clear predominance of elderly patients, with the largest proportion in the 70–79-year group (35.3%), followed by patients aged 60 – 69 years (30.5%) and those older than 80 years (15.9%), while younger patients (<50 years) represented only a small minority (6.0%). These findings are illustrated in Figure 1A, which additionally highlights the sex-specific age distribution.

Baseline serum AFP values (available in 316 patients) showed marked variability (median 11.7 ng/mL, IQR 3.8–284.7). AFP levels increased progressively with pathological tumor stage (Fig. S1), with median concentrations of 5.8 ng/mL (IQR 2.7–21.9) in pT1, 13.3 ng/mL (IQR 3.8–130.8) in pT2, 131.4 ng/mL (IQR 5.5–3925) in pT3, and 7930.0 ng/mL (IQR 172.7–26913.0) in pT4 tumors. In contrast, serum CA19-9 (n = 152), CEA (n = 170), bilirubin, ALT, AST, alkaline phosphatase, and γ-GT showed no clear association with pathological tumor stage, although γ-GT values were numerically higher in pT4 tumors (Figure S1).

Risk factor analysis (Figure 1B) revealed that nearly half of the patients had underlying liver cirrhosis as defined by clinicians (49.7%). Viral hepatitis (HBV/HCV) was present in 24.0% of cases. Metabolic risk factors were also highly prevalent: diabetes mellitus (33.8%), arterial hypertension (45.2%), obesity (18.4%), and metabolic dysfunction–associated steatotic liver disease (MASLD) (4.7%). Steatosis hepatis was documented in 24.3% of patients. Toxic exposures included alcohol consumption in 33.8% and tobacco use in 28.1% of patients. Additionally, esophageal varices were reported in 15.9%.

Tumor staging according to TNM classification showed that most tumors were diagnosed at intermediate stages, with pT2 (35.3%; n = 211) and pT1 (31.3%; n = 187) being the most frequent categories, followed by pT3 (21.1%; n = 126) and pT4 (4.4%; n = 26). Histological grading revealed a predominance of moderately differentiated tumors (G2, 51.3%; n = 306), while well-differentiated (G1; n = 150) and poorly differentiated (G3; n = 117) tumors accounted for 25.1% and 19.6%, respectively (Table 1).

Overall survival (OS) for the entire cohort was 52 months (95% CI 44 – 63 months; n = 597), as depicted in the Kaplan–Meier curve in Figure 1C. In this regard patients with cHCC-CCA (n = 24) showed with 40 months a reduced median overall survival compared to patients with HCC (53 months; n = 573), with no statistically significant difference between the groups (HR 1.34, 95% CI 0.77 – 2.35, $p = 0.2303$). Furthermore, there was no statistically significant difference in our cohort in terms of survival between patients with (n = 297) and without (n = 293) liver cirrhosis (Fig. S3a). Kaplan–Meier analysis showed median OS 53 months of patients with liver cirrhosis. By comparison, with a difference of just one month, mOS was 52 months in patients without liver cirrhosis (HR 0.94, 95% CI 0.75 – 1.17, $p = 0.5518$).

Survival analyses stratified by histological tumor grade (Figure 1D) demonstrated a clear and progressive decline in survival with decreasing differentiation: Patients with G1 tumors showed the longest median overall survival (78 months), followed by those with G2 (55 months) and G3 tumors (32 months). Pairwise comparisons demonstrated a significantly longer overall survival for patients with G1 compared with G3 tumors (78 vs. 32 months, HR 0.52, 95% CI 0.37 – 0.73, $p < 0.0001$) and for patients with G2 compared with G3 tumors (55 vs. 32 months, HR 0.65, 95% CI 0.48 – 0.88, $p = 0.0014$), whereas the difference between G1 and G2 tumors did not reach statistical significance (78 vs. 55 months, HR 0.79, 95% CI 0.61 – 1.04, $p = 0.0989$).

Resection status had a pronounced impact on overall survival (Figure 1E). The majority of patients underwent complete (R0) resection (81.9%, $n = 484$), which was associated with a median overall survival of 63 months. In contrast, patients with microscopic residual disease (R1; 7.4%, $n = 44$) and macroscopic residual disease (R2; 2.5%, $n = 15$) exhibited markedly shorter median overall survival times of 26 and 7 months, respectively. Pairwise comparisons demonstrated statistically significant differences in overall survival between all resection status groups (R0 vs. R1: HR 0.51, 95% CI 0.32 – 0.82, $p = 0.0001$; R0 vs. R2: HR 0.13, 95% CI 0.02 – 0.71, $p < 0.0001$ and R1 vs. R2: HR 0.29, 95% CI 0.10 – 0.87, $p < 0.0001$).

Finally, recurrence rates stratified by resection status (Figure 1F) demonstrated an inverse relationship to overall survival, with increasing recurrence observed in patients with incomplete resections (R1; n = 44 and R2; n = 15). On average, a recurrence was detected after 13 months in R1 cases and as early as 5.5 months in R2 cases. By comparison, the first recurrence in a tumour resected to R0 occurred after 26 months. Significant differences in recurrence rate were observed between R1 and R2 resection status (HR 0.12, 95% CI 0.00 – 30.78, p = 0.0082*)* and R0 (n = 484) and R1 (R0 vs. R1: HR 0.55, 95% CI 0.27 – 1.12, p = 0.0296) whereas no significant difference was detected between R0 and R2 (R0 vs. R2: HR 0.45, 95% CI 0.02 – 8.36, p = 0.4015).

A total of 108 metastatic lesions were documented (Supplementary Fig. S2). The lung represented the most frequent site of metastasis (n = 34), followed by lymph nodes (n = 16), peritoneum (n = 15), bone (n = 13), and other metastatic sites (n = 12). Less common metastatic sites included the adrenal glands (n = 9), liver (n = 5), and, in single cases each, the brain, skin, and pleura (n = 1 each). The site of metastasis was unknown in one patient. Sixty patients (55.6%) presented with a single metastatic site, whereas 34 (31.5%) and 14 patients (13.0%) developed metastases at two and three distinct anatomical sites, respectively.

Characteristic	Value
Total cohort, n (%)	597 (100%)
Age, median (IQR)	
Male	70 (63–77)
Female	67 (57–77)
Age group, n (%)	
<49 years	36 (6.0%)
50–59 years	73 (12.2%)
60–69 years	182 (30.5%)
70–79 years	211 (35.3%)
>80 years	95 (15.9%)
Sex, n (%)	
Male	486 (81.4%)
Female	111 (18.6%)
Tumor markers	
AFP (n=316), mean ± SD; median (IQR)	4608 ng/mL ± 18266; 11.70 (3.8–284.7)
CA 19-9 (n=152), mean ± SD; median (IQR)	26.20 U/mL ± 33.99; 15.20 (9.025–30.30)
CEA (n=170), mean ± SD; median (IQR)	3.009 ng/mL ± 7.861; 1.900 (0.875–3.000)
TNM stage, n (%)	
pT1	187 (31.3%)
pT2	211 (35.3%)
pT3	126 (21.1%)
pT4	26 (4.4%)
Resection status, n (%) / median survival	
R0	484 (81.9%); 63 months
R1	44 (7.4%); 26 months
R2	15 (2.5%); 7 months
Differentiation grade, n (%) / median survival	
G1	150 (25.1%); 78 months

G2	306 (51.3%); 55 months
G3	117 (19.6%); 32 months
Liver disease, n (%)	
Viral hepatitis (B/C)	143 (24.0%)
Cirrhosis	297 (49.7%)
Steatosis hepatis	145 (24.3%)
MASH/MASLD	28 (4.7%)
Comorbidities, n (%)	
Obesity (BMI >30)	110 (18.4%)
Diabetes	202 (33.8%)
Arterial hypertension	270 (45.2%)
Esophageal varices	95 (15.9%)
Toxic exposure, n (%)	
Alcohol consumption*	202 (33.8%)
Tobacco use	168 (28.1%)

Table 1. Baseline patient characteristics and concomitant conditions. Baseline demographic, clinicopathological, and clinical characteristics of the study cohort comprising 597 patients who underwent surgical resection. Age is presented as median and interquartile range (IQR). Tumor marker levels are reported as mean, standard deviation (SD), and IQR. Tumor stage was classified according to the pathological TNM classification (8th edition, UICC/AJCC; 2018). Resection status (R0–R2) and histological differentiation grade (G1–G3) are presented together with median overall survival. Frequencies of underlying liver disease, medication use, comorbidities, and toxic exposures are reported as absolute numbers and percentages. Alcohol consumption was recorded as a binary variable (yes/no), without quantitative assessment of alcohol intake.

Assessment of clinical and pathological prognostic parameters

To identify independent prognostic factors for overall survival (OS), Cox proportional hazards regression analyses were performed using both univariate and multivariate models. The multivariate results are summarized in Table 2, while the full set of univariate analyses is provided in Table S2.

Among patient-related variables, age at diagnosis emerged as a robust and independent prognostic factor. Patients aged ≥60 years had significantly worse survival compared to younger patients in both univariate (HR 1.67, 95% CI 1.31–2.16; $p<0.001$) and multivariate analyses (HR 1.63, 95% CI 1.25–2.16; $p=0.0005$). In contrast, sex had no significant impact on survival (HR 1.04; $p=0.78$, Table S2).

Tumor stage and extent showed a strong and consistent impact on survival. In univariate analysis (Table S2), increasing tumor stage was associated with a stepwise worsening of prognosis, both when comparing grouped T categories (T3–4 vs. T0–2: HR 2.16; p<0.001) and when analyzing individual T stages (e.g., T4 vs. T1: HR 3.51; p<0.001). Similarly, vascular invasion demonstrated a dose-dependent adverse effect (V1 vs. V0: HR 2.01; V2 vs. V0: HR 3.71; both p<0.001), and incomplete resection was associated with markedly reduced survival (R2 vs. R0: HR 6.77; p<0.001). Comparable findings were observed for UICC stage, with progressively increasing hazard ratios from stage II to IV. These key parameters were therefore incorporated into multivariate modeling (Table 2), where advanced tumor stage (HR 1.80; p<0.001), vascular invasion (HR 1.80; p<0.001), and positive resection margins (HR 1.76; p=0.001) remained independent predictors of poor outcome.

Patient-related factors						
Variable	Comparison (reference)	Univariate HR (95% CI)	p value	Multivariate HR (95% CI)	p value	Model
Age at diagnosis	≥60 vs <60 years	1.67 (1.31–2.16)	<0.001	1.63 (1.25–2.16)	0.0005	Model 2
Tumor stage and extent						
T category (combined)	High (T3–4) vs Low (T0–2)	2.16 (1.70–2.73)	<0.001	1.80 (1.40–2.31)	<0.001	Model 2
Vascular invasion (combined)	V+ vs V0	2.17 (1.74–2.72)	<0.001	1.80 (1.41–2.29)	<0.001	Model 5
Resection status (combined)	R+ vs R0	2.31 (1.65–3.17)	<0.001	1.76 (1.24–2.44)	0.001	Model 2
Tumor morphology and histopathology						
Tumor grading (collapsed)	G3–4 vs G1–2	1.81 (1.31–2.51)	<0.001	35.4 (1.95–174.6)	0.0006	Model 2
MTM subtype	MTM vs non-MTM	2.95 (1.51–5.16)	0.001	2.92 (1.49–5.13)	0.0006	Model 1
Tumor capsule	Present vs Absent	0.63 (0.46–0.91)	0.009	0.56 (0.40–0.80)	0.001	Model 5
Background liver disease						
Steatosis	Yes vs No	0.80 (0.64–1.00)	0.048	0.72 (0.56–0.93)	0.014	Model 4
Liver cirrhosis	Yes vs No	0.94 (0.76–1.15)	0.53	—	—	—
Comorbidities						
Diabetes mellitus	Yes vs No	1.37 (1.09–1.73)	0.008	1.20 (0.94–1.54)	0.15	Model 4
Chronic hepatitis (B/C)	Yes vs No	0.74 (0.57–0.95)	0.023	—	—	—
Laboratory parameters						
AFP	Elevated vs Normal	1.58 (1.17–2.14)	0.003	1.52 (0.87–2.65)	0.14	Model 4
Alkaline phosphatase	Elevated vs Normal	1.95 (1.44–2.66)	<0.001	1.79 (1.04–3.13)	0.037	Model 4
GOT	Elevated vs Normal	1.48 (1.09–2.00)	0.012	1.56 (0.86–2.79)	0.14	Model 4

Table 2. Cox regression analysis for overall survival**.** Event: death; method: Cox proportional hazards regression; n varies due to missing data (available-case analysis). Model 1 – Histological subtype model

Included variables: MTM subtype and T category (combined).

Model 2 – Core clinicopathological model

Included variables: age at diagnosis, T category (combined), vascular invasion, resection margin status, and tumor grading.

Model 3 – Molecular/IHC model

Included variables: age at diagnosis, p53 (IHC), Cyclin A2 and/or Cyclin E1, and T category (combined).

Model 4 – Clinical–laboratory model

Included variables: age at diagnosis, steatosis, diabetes mellitus, AFP, alkaline phosphatase, and GOT.

Model 5 – Tumor architecture model

Included variables: tumor capsule, vascular invasion, and T category (combined).

Tumor morphology and histopathological features were extensively assessed in the univariate analysis (Table S2). Poor tumor differentiation (G3–4 vs. G1–2) was significantly associated with worse survival.

Among histological subtypes, only the macrotrabecular–massive (MTM) subtype showed a significant adverse prognostic impact (HR 2.95; p=0.001), whereas other architectural patterns - including trabecular, pseudoglandular, microtrabecular, steatohepatitic, clear cell, chromophobe, fibrolamellar, and lymphocyte-rich variants - did not reach statistical significance. This selective significance of the MTM subtype explains the subsequent focus on this entity in multivariate modeling (Model 1, Table 2), where it remained independently associated with poor survival (HR 2.92; p=0.0006).

Additional histopathological parameters analyzed in Table S2 included the presence of Mallory hyaline, tumor capsule, and tumoral cholestasis. Among these, only the presence of a tumor capsule was significantly associated with improved survival (HR 0.63; p=0.009), an effect that persisted in multivariate analysis (HR 0.56; p=0.001). In contrast, Mallory hyaline and tumoral cholestasis showed no prognostic relevance.

Background liver disease and microenvironmental features were also evaluated. Neither liver cirrhosis nor Ishak fibrosis stage nor inflammatory activity showed a significant impact on survival in univariate analysis (Table S2).It should be noted that a certain bias could be introduced with respect to liver cirrhosis, due to the fact that only resected specimens were included and higher liver cirrhosis levels might have prevented surgical resection in patients that were thus not included to the study. However,

the presence of steatosis was associated with improved survival (HR 0.80; p=0.048), and this effect remained significant in multivariate analysis (HR 0.72; p=0.014).

With regard to comorbidities and metabolic factors, univariate analysis (Table S2) revealed that diabetes mellitus (HR 1.37; p=0.008) and arterial hypertension (HR 1.29; p=0.034) were associated with worse survival. However, only diabetes mellitus was carried forward into multivariate analysis, where it did not retain statistical significance (HR 1.20; p=0.15). Other factors, including alcohol abuse, nicotine use, drug abuse, obesity, and BMI as a continuous variable, showed no significant association with survival. Interestingly, chronic viral hepatitis (HBV/HCV) was associated with improved survival in univariate analysis (HR 0.74; p=0.023), although this was not confirmed in multivariate modeling.

Laboratory parameters were likewise evaluated in detail (Table S2). Elevated AFP levels were associated with worse survival in univariate analysis (HR 1.58; p=0.003), but this effect did not persist after adjustment (HR 1.52; p=0.14). Elevated CA 19-9 and γ-GT levels were also associated with worse survival in univariate analysis, whereas CEA, bilirubin, INR, and Quick values showed no significant associations. Notably, elevated alkaline phosphatase emerged as a consistent and independent adverse prognostic factor, remaining significant in both univariate (HR 1.95; p<0.001) and multivariate analyses (HR 1.79; p=0.037). Elevated GOT (AST) levels were associated with worse survival in univariate analysis (HR 1.48; p=0.012), but did not retain significance in multivariate analysis.

For multivariate modeling, variables were primarily selected based on their significance in univariate analysis (Table S2) and clinical relevance. Several models were constructed (Table 2), including a histological subtype model (Model 1), a core clinicopathological model (Model 2), and additional models integrating clinical and laboratory variables. Across these models, age, tumor stage, vascular invasion, resection margin status, tumor grading, MTM subtype, tumor capsule, steatosis, and alkaline phosphatase emerged as the most robust determinants of survival.

Evaluation potential of immunohistochemistry molecular surrogates for HCC substratification

To further refine tumor stratification beyond conventional clinicopathological parameters, we evaluated a panel of immunohistochemical (IHC) markers as surrogate readouts for underlying molecular alterations using tissue microarrays (TMAs). The analyzed markers included L-FABP1, β-catenin, p53, Cyclin A2, and Cyclin E1, all of which have previously been linked to specific molecular pathways in hepatocarcinogenesis.

Representative staining patterns for all markers are shown in Figure 2A. L-FABP1 expression was assessed as retained versus lost, serving as a surrogate for HNF1A alterations. β-catenin staining was evaluated with respect to subcellular localization, distinguishing membranous expression from nuclear accumulation, the latter reflecting activation of the Wnt/β-catenin pathway and possibly underlying mutations of APC or β-catenin. For p53, evaluation of a complete loss (“null pattern”) was not feasible due to generally low baseline expression in both tumor and non-neoplastic liver tissue. Therefore, p53 status was assessed using an H-score–based approach, and tumors with an H-score ≥150 were

classified as “p53 high,” representing a surrogate for TP53 mutation. Cyclin A2 and Cyclin E1 expression were likewise quantified using H-scores, with a predefined cutoff of ≥100 to define “high” expression. Given the low absolute frequency of high expression for each marker individually and their biological similarity, Cyclin A2 and Cyclin E1 were additionally combined into a joint category (Cyclin A2/E1 high).

Quantitative assessment of these markers is summarized in Figure 2C. p53 high expression was observed in 23 of 417 evaluable samples (5.5%). Cyclin A2 high expression was rare (7/418 cases, 1.7%), as was Cyclin E1 high expression (13/413 cases, 3.1%). Combined Cyclin A2/E1 high status was present in 19 cases (3.4%). For β-catenin (Figure 2D), nuclear localization was identified in 30 of 416 cases (7.2%), while the majority showed membranous staining. L-FABP1 loss was detected in 30 cases, whereas 385 cases retained expression.

A particularly notable observation was the identification of a rare “double phenotype” combining p53 high expression and nuclear β-catenin localization, corresponding to concurrent activation of TP53 and Wnt/β-catenin pathways. This phenotype was observed in only a single case within the cohort. Histologically, this tumor had a low differentiation grade and exhibited an aggressive clinical course with very short overall survival. The corresponding IHC findings are illustrated in Figure 2B.

Survival analyses based on IHC-defined subgroups are shown in Figures 2E and 2F. Patients with p53 high tumors had significantly worse overall survival compared to those with p53 low tumors (Figure 2E). Similarly, tumors with high Cyclin A2/E1 expression were associated with significantly reduced survival (Figure 2F), as assessed by Kaplan–Meier analysis and log-rank testing.

These findings were further supported by Cox regression analyses summarized in Table 3. In univariate analysis, p53 high expression was significantly associated with worse survival (HR 1.91, 95% CI 1.14–3.01; p=0.008). Importantly, this association remained significant in multivariate analysis within Model 3 (HR 1.80, 95% CI 1.03–2.96; p=0.028), indicating that p53 IHC status represents an independent prognostic factor when adjusted for age and tumor stage. On closer inspection, TP53-high tumors (H-score ≥ 150), 66.7% (12/18) were poorly differentiated (G3), whereas 27.8% (5/18) were G2 and only 5.6% (1/18) were G1. Cyclin A2/E1 high expression was also significantly associated with worse survival in univariate analysis (HR 2.27, 95% CI 1.26–3.76; p=0.003), but did not retain statistical significance in multivariate analysis (HR 1.68, 95% CI 0.85–2.98; p=0.099), suggesting a potential effect, which in this series could not be proven to be independent.

Variable	Comparison (reference)	Univariate HR (95% CI)	p value	Multivariate HR (95% CI)	p value	Model
p53 (IHC, H-score)	High (≥150) vs Low	1.91 (1.14–3.01)	0.008	1.80 (1.03–2.96)	0.028	Model 3
Cyclin A2 and/or Cyclin E1	High (≥100) vs Low	2.27 (1.26–3.76)	0.003	1.68 (0.85–2.98)	0.099	Model 3
L-FABP1	Loss vs Retained	1.22 (0.79–1.81)	0.34	—	—	—
β-Catenin	Nuclear vs Non-nuclear	1.28 (0.78–1.97)	0.30	—	—	—

Table 3. Cox regression analysis for overall survival- molecular/ immunohistochemical markers**.** Event: death; method: Cox proportional hazards regression; n varies due to missing data (available-case analysis).

Model 3 – Molecular/IHC model

Included variables: age at diagnosis, p53 (IHC), Cyclin A2 and/or Cyclin E1, and T category (combined).

In contrast, L-FABP1 loss and nuclear β-catenin expression were not associated with overall survival (HR 1.22, p=0.34 and HR 1.28, p=0.30, respectively) and were therefore not included in multivariate models.

Taken together, these results demonstrate that selected immunohistochemical markers, particularly p53 overexpression, can provide additional prognostic information beyond standard clinicopathological parameters. While Cyclin A2/E1 expression shows a trend toward prognostic relevance, its independent value appears limited. Other markers such as L-FABP1 and β-catenin, although biologically informative, did not show prognostic significance in this cohort.

Clinical outcome parameters with respect to systemic treatment

Clinical outcome parameters with regard to systemic therapies were evaluated in a subset of patients with available follow-up and treatment response data. The results are summarized in Figure 3.

Therapy response rates for the most frequently used first-line regimens are shown in Figure 3A. Among patients treated with atezolizumab plus bevacizumab (n = 26), one patient achieved complete remission, eight showed partial remission, one had a mixed response, eight had stable disease, and eight experienced progressive disease. In contrast, patients treated with sorafenib as first-line therapy (n = 22) did not show any complete responses; four patients achieved partial remission, two had mixed response, two had stable disease, and the majority (n = 14) exhibited progressive disease. For lenvatinib, response assessment was available in only a small number of patients (n = 4), all of whom demonstrated progressive disease, indicating limited efficacy in this small subgroup.

Progression-free survival (PFS) in the first line setting is illustrated in Figure 3B. The largest cohorts were observed for atezolizumab/bevacizumab (n = 35) and sorafenib (n = 44), followed by lenvatinib (n = 11), durvalumab/tremelimumab (n = 5), and cabozantinib (n = 2). Kaplan–Meier analysis demonstrated median progression-free survival (mPFS) was longest in patients treated with atezolizumab plus bevacizumab (270 days), followed by sorafenib (258 days), lenvatinib (94 days), durvalumab plus tremelimumab (88.5 days), and cabozantinib (21.5 days). Pairwise comparisons were performed using the log-rank test and demonstrated no significant difference in mPFS between atezolizumab plus bevacizumab and sorafenib (270 vs. 258 days; HR 0.62, 95% CI 0.31 – 1.25, $p = 0.1554$). Median PFS was numerically longer in patients treated sorafenib than in those receiving lenvatinib (258 vs. 94 days); however, this difference did not reach statistical significance (HR 0.49, 95% CI 0.12 – 1.99, $p = 0.1715$). In contrast, atezolizumab plus bevacizumab was associated with significantly longer mPFS than lenvatinib (270 vs. 94 days; HR 0.28, 95% CI 0.05 – 1.65, $p = 0.0120$), durvalumab plus tremelimumab (270 vs. 88.5 days; HR 0.18, 95% CI 0.01 – 4.21, $p = 0.0078$), and cabozantinib (270 vs. 21.5 days; HR 0.05, 95% CI 0.00 – 17.21, $p < 0.0001$). Because of the small sample size and substantial censoring, hazard ratio estimates were unstable and should be interpreted with caution.

Following the analysis of first-line treatment outcomes, progression-free survival was also displayed with Kaplan-Meier graphs for the most frequently administered second-line systemic therapies (Supplementary Fig. S4). Visually Atezolizumab and bevacizumab were also superior in this setting. However no statistics were performed due to the small numbers of patients.

The sequential use of systemic therapies is depicted in an alluvial plot in Figure 3C, illustrating treatment lines over time. Sorafenib was the most frequently administered first-line therapy (n=44), followed by atezolizumab/bevacizumab (n=35), reflecting changes in therapeutic standards over the study period. Additional first-line treatments included lenvatinib (n=11), durvalumab/tremelimumab (n=5), cabozantinib (n=2), and atezolizumab monotherapy (n=2).

In the second-line setting, the majority of patients (n=60) did not receive further systemic therapy, due to a combination of factors including disease progression, clinical deterioration, or loss to follow-up. Among those who continued treatment, a heterogeneous distribution of regimens was observed, including repeated or continued use of atezolizumab/bevacizumab in a subset of patients. Subsequent therapy lines (third and beyond) demonstrated increasing heterogeneity, with only a small number of patients receiving later-line treatments.

Notably, a single young patient with underlying liver fibrosis resulting from chronic Hepatitis B underwent an extensive sequence of systemic therapies up to sixth-line treatment. This patient received atezolizumab/bevacizumab (first line) sorafenib (second line), ramucirumab (third line), cabozantinib (fourth line), ipilimumab/nivolumab and 39 cycles nivolumab monotherapy (fifth line), and lenvatinib (sixth line). While most treatment regimens resulted in progressive disease (pd) as the best overall response, prolonged disease stabilization (sd) was achieved during nivolumab maintenance therapy (39 cycles) and subsequently with Lenvatinib.

A small subgroup of patients (*n* = 29) received best supportive care (BSC). As shown in Figure S3b, median OS in this cohort was 34 days (95% CI, 11 – 86 days).

Discussion

This retrospective single-center study provides a comprehensive clinicopathological analysis of HCC over a 25-year period and captures the evolution of diagnostic, prognostic, and therapeutic aspects of the disease in a large real-world cohort from Eastern Bavaria. Several findings deserve emphasis. First, the cohort reflects the well-established epidemiological profile of HCC in a European population, with a clear male predominance and a peak incidence in older patients. Second, survival was primarily driven by classical clinicopathological features, especially tumor stage, vascular invasion, resection status, and grading. Third, selected histological and immunohistochemical subclassification approaches added further prognostic information, particularly the identification of the macrotrabecular-massive subtype and p53-high tumors. Finally, the treatment analyses document the shift from tyrosine kinase inhibitor-based therapy to immune checkpoint inhibitor-based regimens in real-world clinical practice.

The baseline characteristics of our cohort are in line with the known epidemiology of HCC [20]. Male patients accounted for more than 80% of cases, which is consistent with the reported sex disparity in HCC incidence. Likewise, cirrhosis, viral hepatitis, alcohol-associated liver disease, and metabolic comorbidities were all common in our cohort. Particularly noteworthy is the substantial burden of metabolic risk factors such as diabetes, obesity, hypertension, and steatosis. This pattern mirrors the ongoing epidemiological shift observed in Western countries, where MASLD/MASH-related hepatocarcinogenesis is gaining importance [21]. At the same time, the relatively high prevalence of viral hepatitis and cirrhosis indicates that classic etiologic drivers remain highly relevant in a Central European tertiary care cohort.

As expected, conventional pathological staging parameters were among the strongest prognostic determinants. Higher T category, vascular invasion, and positive resection margin status were all independently associated with worse overall survival. These findings confirm that tumor burden and local tumor spread remain central determinants of clinical outcome. Similarly, incomplete resection was associated with markedly shorter survival and higher recurrence rates, underscoring the importance of radical surgery whenever feasible. Histological grading also showed the anticipated stepwise association with prognosis, with poorer differentiation corresponding to reduced survival. Together, these data confirm that established morphological parameters remain highly informative and retain major prognostic value despite the emergence of molecular and therapeutic stratification approaches.

Among histological subtypes, only the macrotrabecular-massive subtype showed a clear and independent association with worse overall survival. This is well in line with previous studies linking MTM-HCC to aggressive biological behavior, elevated AFP levels, vascular invasion, and TP53 alterations [22]. In contrast, the other recognized histological variants did not demonstrate prognostic significance in our cohort. This may partly reflect the limited case numbers for rarer subtypes, which restrict

statistical power in retrospective real-world series. Nevertheless, the clear signal for MTM-HCC supports the relevance of subtype-aware histopathological classification in routine reporting, at least for this aggressive variant.

An additional morphological feature with prognostic relevance in our study was the presence of a tumor capsule, which was associated with improved survival in both univariate and multivariate analyses. This finding is biologically plausible, as encapsulated tumors may reflect a less infiltrative growth pattern and lower invasive potential. In contrast, other histological features such as Mallory hyaline or tumoral cholestasis did not show significant associations with survival. These results suggest that not all descriptive morphological features are equally informative from a prognostic perspective, and that future pathology reporting might benefit from prioritizing those parameters that consistently translate into clinically relevant risk stratification.

The analysis of background liver pathology yielded some interesting observations. While cirrhosis itself was not associated with survival in our cohort (while a certain bias could exist with the preselection of patients undergoing resection compared to unresected patients who tend to have a highter lever of cirrhosis), steatosis showed an association with better outcome. This finding should be interpreted cautiously. On the one hand, it may point toward biological differences between steatotic and non-steatotic tumors or reflect differences in underlying disease trajectories. On the other hand, it may also be influenced by confounding factors, including differences in surveillance intensity, treatment allocation, or competing risk structures across etiologic subgroups. Similarly, chronic viral hepatitis was associated with improved survival in univariate analysis, which may reflect closer surveillance or earlier-stage diagnosis in these patients rather than a direct biological advantage.

A major aim of this study was to explore whether immunohistochemical surrogate markers could be used for a pragmatic molecular subclassification of HCC in routine pathology. In this regard, p53 overexpression emerged as the most relevant marker. Tumors with high p53 H-score had significantly worse overall survival, and this association remained significant in multivariate analysis. This supports the idea that p53 immunohistochemistry can capture biological differences in HCC, even though it is an imperfect surrogate for TP53 mutation status. Notably, we did not assess a p53-null pattern as a separate category, because very low or absent p53 expression was common in both tumor and surrounding liver tissue and therefore not sufficiently discriminatory in this tumor type and not assessible by TMA. Our H-score-based strategy therefore focused on a clearly aberrant overexpression phenotype.

Combined high expression of Cyclin A2 and/or Cyclin E1 was associated with worse survival in univariate analysis, but this effect did not remain statistically significant in the multivariate model. An additional analysis in larger cohorts appears warranted. This suggests that Cyclin A2/E1 expression may reflect aggressive tumor biology, but that its prognostic effect overlaps with established clinicopathological features such as age and tumor stage. Nevertheless, the association is biologically plausible and consistent with previous work linking dysregulated cell-cycle proteins to tumor progression

[23]. In contrast, L-FABP1 loss and nuclear β-catenin expression were not prognostic in our cohort. This suggests that their utility may be more important in diagnostic subclassification or pathway annotation than in direct prognostic prediction.

A particularly intriguing finding was the identification of a single tumor showing concomitant p53 overexpression and nuclear β-catenin accumulation. This rare double-positive phenotype may correspond to a molecularly unusual subgroup with combined TP53 and CTNNB1 pathway alterations, reminiscent of recently proposed dual-pathway constellations [11]. Although represented by only one case in our series, the unusually aggressive clinical course of this patient is notable. At the same time, caution is warranted, as immunohistochemistry can only approximate underlying molecular events and will inevitably miss cases without overt protein-level surrogates.

Our evaluation of systemic therapy outcomes reflects the changing therapeutic landscape in HCC over the last decade [14]. Sorafenib represented the most common first-line therapy overall, which is expected given its long-standing role as the standard systemic option prior to the immunotherapy era. More recently, atezolizumab plus bevacizumab became increasingly relevant and showed the most favorable response pattern in our cohort, including one complete remission and several partial remissions. Progression-free survival also appeared longest in the atezolizumab/bevacizumab group, although sorafenib showed partly comparable curves in this retrospective analysis. These observations are directionally in line with the pivotal trial data [24], but should be interpreted cautiously because of limited subgroup sizes, treatment-era effects, and inherent biases of retrospective non-randomized datasets. The poor outcomes observed in the small lenvatinib and durvalumab/tremelimumab groups likely reflect both small sample size and selection effects, rather than allowing definitive comparative conclusions. A similar pattern was observed forsecond-line therapy. Although a significant result was observed for atezolizumab/bevacizumab versus sorafenib, given the small size of the cohort, this should only be regarded as a hypothesis-generating outcome and was therefore underpowered to draw robust conclusions.

The treatment-sequence analysis further emphasizes the heterogeneity of real-world HCC management. While many patients did not receive second-line therapy, a subset underwent complex multi-line treatment courses. The identification of one patient who received up to six lines of therapy is particularly illustrative and highlights the expanding range of therapeutic options for selected patients with preserved performance status.

Several limitations of this study should be acknowledged. The retrospective single-center design entails inherent risks of selection bias, incomplete data capture, and heterogeneity in diagnostic work-up and treatment over time. Missing data affected some laboratory and clinical variables, and sample sizes for selected subgroups, particularly rare histological variants and newer systemic therapies, were limited. In addition, the long study period necessarily spans major changes in staging systems, surgical strategies, systemic therapies, and follow-up routines. The immunohistochemical analyses were performed on

tissue microarrays and this may not fully capture intratumoral heterogeneity. Moreover, the analyzed IHC markers represent surrogate rather than direct molecular readouts.

In conclusion, this study confirms the major prognostic relevance of established clinicopathological factors in HCC while also demonstrating that selected histological and immunohistochemical features provide additional stratification value. In particular, the MTM subtype and p53 overexpression identify clinically unfavorable tumor subsets, whereas tumor capsule and steatosis were associated with more favorable outcome. The treatment analyses reflect the real-world transition from sorafenib-based therapy to immunotherapy-based regimens. Taken together, our findings support an integrated pathology-centered approach to HCC characterization that combines conventional morphology, selected immunohistochemical surrogate markers, and clinical context in order to improve risk stratification.

Conclusions

In this quarter-century single-center cohort, overall survival in hepatocellular carcinoma was primarily determined by established clinicopathological parameters, particularly tumor stage, vascular invasion, resection status, and grading. In addition, the macrotrabecular-massive subtype and p53 overexpression identified biologically aggressive subgroups with adverse outcome, supporting the added value of refined histopathological and immunohistochemical stratification. Finally, the systemic therapy data reflect the major therapeutic transition from sorafenib-based treatment toward immunotherapy-based regimens in real-world clinical practice.

Abbreviations

AFP: alpha-fetoprotein

AJCC: American Joint Committee on Cancer

ALT: alanine aminotransferase

AST: aspartate aminotransferase

Atezo/Bev: atezolizumab plus bevacizumab

BAP1: BRCA1-associated protein 1

BMI: body mass index

BSC: best supportive care

CA 19-9: carbohydrate antigen 19-9

CAF: cancer-associated fibroblast

CCNA2: cyclin A2

CCNE1: cyclin E1

CEA: carcinoembryonic antigen

cHCC-CCA: combined hepatocellular–cholangiocarcinoma

CI: confidence interval

CR: complete response

CTNNB1: catenin beta 1

DAB: 3,3'-diaminobenzidine

FDA: U.S. Food and Drug Administration

FFPE: formalin-fixed, paraffin-embedded

FLC: fibrolamellar carcinoma

GOT: glutamate oxaloacetate transaminase

GPT: glutamate pyruvate transaminase

γ-GT: gamma-glutamyltransferase

HBV: hepatitis B virus

HCC: hepatocellular carcinoma

HCV: hepatitis C virus

H&E: hematoxylin and eosin

HNF1A: hepatocyte nuclear factor 1 alpha

HR: hazard ratio

HRP: horseradish peroxidase

IHC: immunohistochemistry

INR: international normalized ratio

IQR: interquartile range

IRF2: interferon regulatory factor 2

L-FABP1: liver fatty acid-binding protein 1

MASLD: metabolic dysfunction–associated steatotic liver disease

MASH: metabolic dysfunction–associated steatohepatitis

MR: mixed response

MTM: macrotrabecular-massive

MTM-HCC: macrotrabecular-massive hepatocellular carcinoma

NOS: not otherwise specified

OS: overall survival

PD: progressive disease

PFS: progression-free survival

PR: partial response

R0: microscopically margin-negative resection

R1: microscopically margin-positive resection

R2: macroscopically incomplete resection

SD: stable disease

SH-HCC: steatohepatitic hepatocellular carcinoma

TACE: transarterial chemoembolization

TERT: telomerase reverse transcriptase

TMA: tissue microarray

TKI: tyrosine kinase inhibitor

TNM: tumor–node–metastasis

UICC: Union for International Cancer Control

WHO: World Health Organization

Declarations

Ethics approval and consent to participate

Data collection and analysis were conducted in accordance with applicable data protection regulations. Due to the retrospective study design, the requirement for individual informed consent was waived. All data were analyzed in anonymized form.

Competing Interests

The authors declare the following competing interests:KU: received honoraria from Roche, BMS, Lilly, AMGEN, Minarini Stemline.

Funding

No grant support has been obtained for this project. No external funding has been obtained. Only regular intramural funding by the university administration was employed for the project.

Author Contribution

Conceptualization: KE, KU, SS, AS; Methodology: SS, KU, KE, AS; Software: SS, AS; Validation: SS, AS, KE, KU; Formal analysis: SS, AS; Investigation; KE, KU, AS, SS, EP, MV, PK, TG, BL, PH, AK, Monika Kerscher; Resources: ME, DC; Data curation: AS, KE, SS, KU; Writing – original draft: AS, SS; Writing – review & editing: all authors; Visualization: SS, AS; Supervision: KE, ME, DC; Project administration: KE, ME; Funding acquisition: ME (internal institutional fundings). All authors have read and approved the final version of this manuscript.

Acknowledgement

We thank our laboratory assistants Monika Kerscher, Ingrid Winkel and Manfred Meyer, for their invaluable support throughout the project. The authors would like to thank Mr. Armin Pauer (Tumor Center - Institute for Quality Management and Health Services Research, University of Regensburg) for his support in obtaining patient survival and treatment data from the local cancer registry. For additional proofreading and enhancing linguistic clarity of the manuscript, the large language model ChatGPT (Version 5, OpenAI, San Francisco, CA, USA) was utilized.References

Data Availability

The datasets supporting the conclusions of this article are included within the article. Moreover anonymized collated data may be shared upon reasonable request.

References

1. Liver EA for the S of the, Sangro B, Argemi J, Ronot M, Paradis V, Meyer T et al. EASL Clinical Practice Guidelines on the management of hepatocellular carcinoma. J Hepatol. 2025;82:315–74.
2. Llovet JM, Kelley RK, Villanueva A, Singal AG, Pikarsky E, Roayaie S, et al. Hepatocellular carcinoma. Nat Rev Dis Prim. 2021;7:6.
3. Soerjomataram BJ, Siegel I, Torre RL, Jemal LA, Ahmedin FF. Global cancer statistics 2018: GLOBOCAN estimates of incidence and mortality worldwide for 36 cancers in 185 countries. CA Cancer J Clin. 2018;68:394–424.
4. Valery PC, Laversanne M, Clark PJ, Petrick JL, McGlynn KA, Bray F. Projections of primary liver cancer to 2030 in 30 countries worldwide. Hepatology. 2018;67:600–11.
5. Rumgay H, Arnold M, Ferlay J, Lesi O, Cabasag CJ, Vignat J, et al. Global burden of primary liver cancer in 2020 and predictions to 2040. J Hepatol. 2022;77:1598–606.
6. Lee HA. Pathogenesis and management of metabolic dysfunction-associated steatohepatitis-related hepatocellular carcinoma: a narrative review. Ewha Med J. 2024;47.
7. Arends MJ, Esposito I, Gill AJ, Hruban RH, Khoury JD, Kojima M, et al. Changes in the 6th edition of the World Health Organization classification of tumours of the digestive system. Histopathology. 2026;88:1295–314.
8. Shin SH, Park JY, Hwang C, Lee HJ, Shin DH, Kim JY, et al. Histological subtypes of hepatocellular carcinoma: Their clinical and prognostic significance. Ann Diagn Pathol. 2023;64:152134.
9. Kim H, Jang M, Park YN. Histopathological Variants of Hepatocellular Carcinomas: an Update According to the 5th Edition of the WHO Classification of Digestive System Tumors. J Liver Cancer. 2020;20:17–24.
10. Selene II, Ozen M, Patel RA. Hepatocellular Carcinoma: Advances in Systemic Therapy. Semin Intervent Radiol. 2024;41:56.
11. Pan L, Hirsch TZ, Fang J, Seretny A, Imbeaud S, Jin S, et al. Integrated genomic analyses identify oncogenic pathway interplay in hepatocarcinogenesis defining specific molecular subtypes. Nat Commun. 2026. https://doi.org/10.1038/s41467-026-73212-y.
12. Ferrante ND, Pillai A, Singal AG. Update on the Diagnosis and Treatment of Hepatocellular Carcinoma. 506 Gastroenterol Hepatol. 2020;16.
13. Llovet JM, Ricci S, Mazzaferro V, Hilgard P, Gane E, Blanc J-F, et al. Sorafenib in Advanced Hepatocellular Carcinoma. N Engl J Med. 2008;359:378–90.
14. Ben Khaled N, Mörtl B, Beier D, Reiter FP, Pawlowska-Phelan D, Teufel A et al. Changing treatment landscape associated with improved survival in advanced hepatocellular carcinoma: a nationwide, population-based study. Eur J Cancer. 2023;192.

15. Finn RS, Qin S, Ikeda M, Galle PR, Ducreux M, Kim T-Y et al. IMbrave150: Updated overall survival (OS) data from a global, randomized, open-label phase III study of atezolizumab (atezo) + bevacizumab (bev) versus sorafenib (sor) in patients (pts) with unresectable hepatocellular carcinoma (HCC). J Clin Oncol. 2021;39 3_suppl:267.
16. Hwang SY, Danpanichkul P, Agopian V, Mehta N, Parikh ND, Abou-Alfa GK, et al. Hepatocellular carcinoma: updates on epidemiology, surveillance, diagnosis and treatment. Clin Mol Hepatol. 2025;31(Suppl):S228–54.
17. McCarty KSJ, Szabo E, Flowers JL, Cox EB, Leight GS, Miller L, et al. Use of a monoclonal anti-estrogen receptor antibody in the immunohistochemical evaluation of human tumors. Cancer Res. 1986;46(8 Suppl):s4244–8.
18. Bioulac-Sage P, Rebouissou S, Thomas C, Blanc J-F, Saric J, Sa Cunha A, et al. Hepatocellular adenoma subtype classification using molecular markers and immunohistochemistry. Hepatology. 2007;46:740–8.
19. de La Coste A, Romagnolo B, Billuart P, Renard CA, Buendia MA, Soubrane O, et al. Somatic mutations of the beta-catenin gene are frequent in mouse and human hepatocellular carcinomas. Proc Natl Acad Sci U S A. 1998;95:8847–51.
20. Sung H, Ferlay J, Siegel RL, Laversanne M, Soerjomataram I, Jemal A, et al. Global Cancer Statistics 2020: GLOBOCAN Estimates of Incidence and Mortality Worldwide for 36 Cancers in 185 Countries. CA Cancer J Clin. 2021;71:209–49.
21. Leyh C, Coombes JD, Schmidt HH, Canbay A, Manka PP, Best J. MASLD-Related HCC-Update on Pathogenesis and Current Treatment Options. J Pers Med. 2024;14.
22. Sessa A, Mulé S, Brustia R, Regnault H, Galletto Pregliasco A, Rhaiem R et al. Macrotrabecular-Massive Hepatocellular Carcinoma: Light and Shadow in Current Knowledge. J Hepatocell Carcinoma. 2022;9 null:661–70.
23. Bayard Q, Meunier L, Peneau C, Renault V, Shinde J, Nault J-C, et al. Cyclin A2/E1 activation defines a hepatocellular carcinoma subclass with a rearrangement signature of replication stress. Nat Commun. 2018;9:5235.
24. ; Finn Shukui, Ikeda M, Galle PR, Ducreux M, Kim T-Y, Lim HY, Kudo M, Breder V, Merle P, Kaseb A, Li D, Verret W, Shao H, Liu J, Li L, Zhu AX, Cheng, Ann-Lii RS. Q. IMbrave150: Updated overall survival (OS) data from a global, randomized, open-label phase III study of atezolizumab (atezo) + bevacizumab (bev) versus sorafenib (sor) in patients (pts) with unresectable hepatocellular carcinoma (HCC). J Clin Oncol. 2021;39 3_suppl:267.

Figures

Figure 1

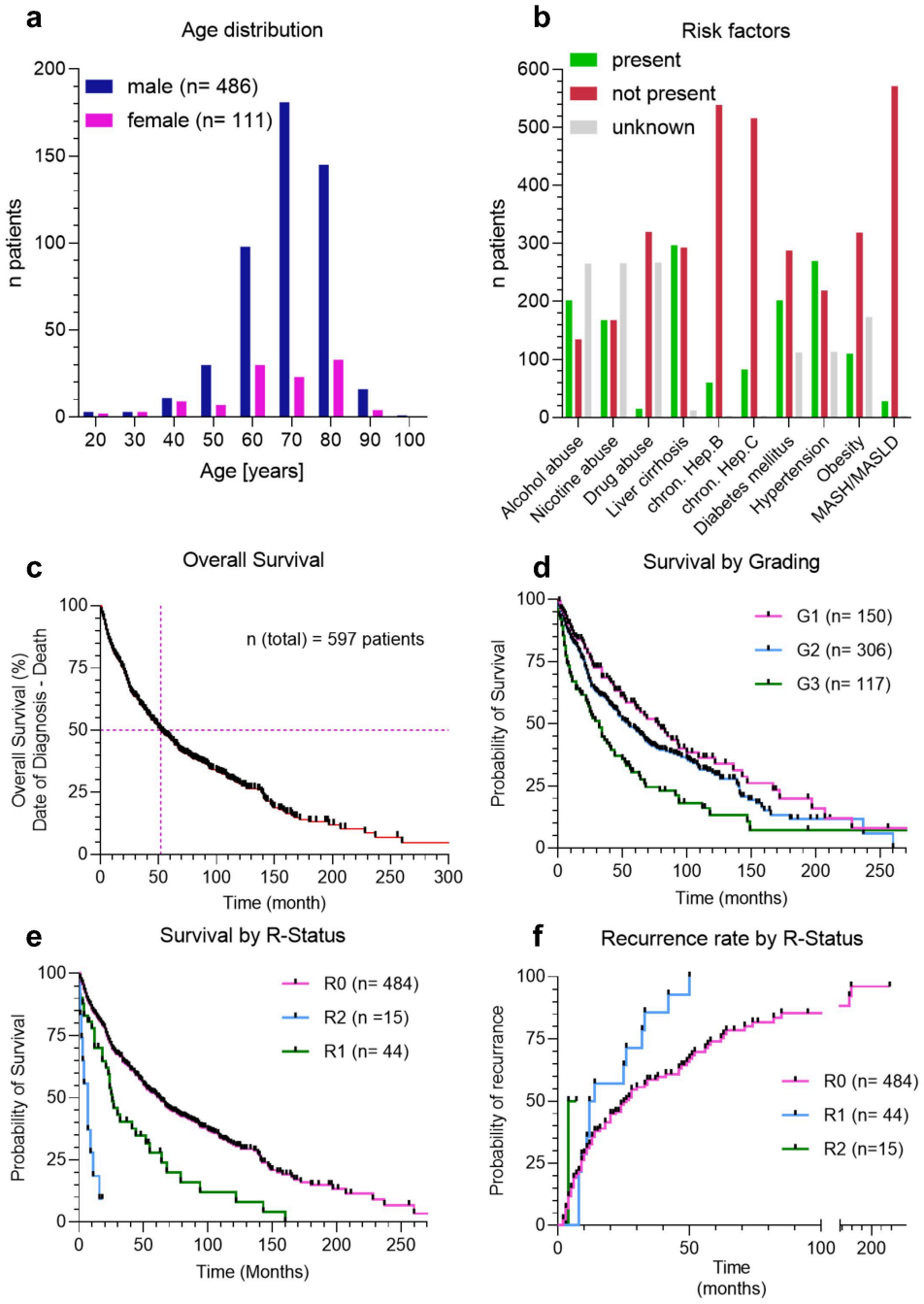


Figure 1

Clinicopathological characteristics and survival analyses of patients with hepatocellular carcinoma. **(A)** Age distribution of patients stratified by sex, shown as bar charts across defined age intervals; male and female patients are indicated by color. **(B)** Distribution of underlying risk factors, categorized as present, absent, or unknown, displayed as absolute patient numbers. **(C)**Overall survival of the entire cohort (n = 597), shown as a Kaplan–Meier curve with median overall survival indicated in months. **(D)** Overall

survival stratified by histological grading (G1, G2, G3), presented as Kaplan–Meier curves with time given in months. **(E)** Overall survival according to resection status (R0, R1, R2), shown as Kaplan–Meier curves. **(F)**Recurrence-free survival according to resection status (R0, R1, R2), presented as Kaplan–Meier curves indicating the probability of recurrence over time (months); tick marks denote censored observations.

Figure 2

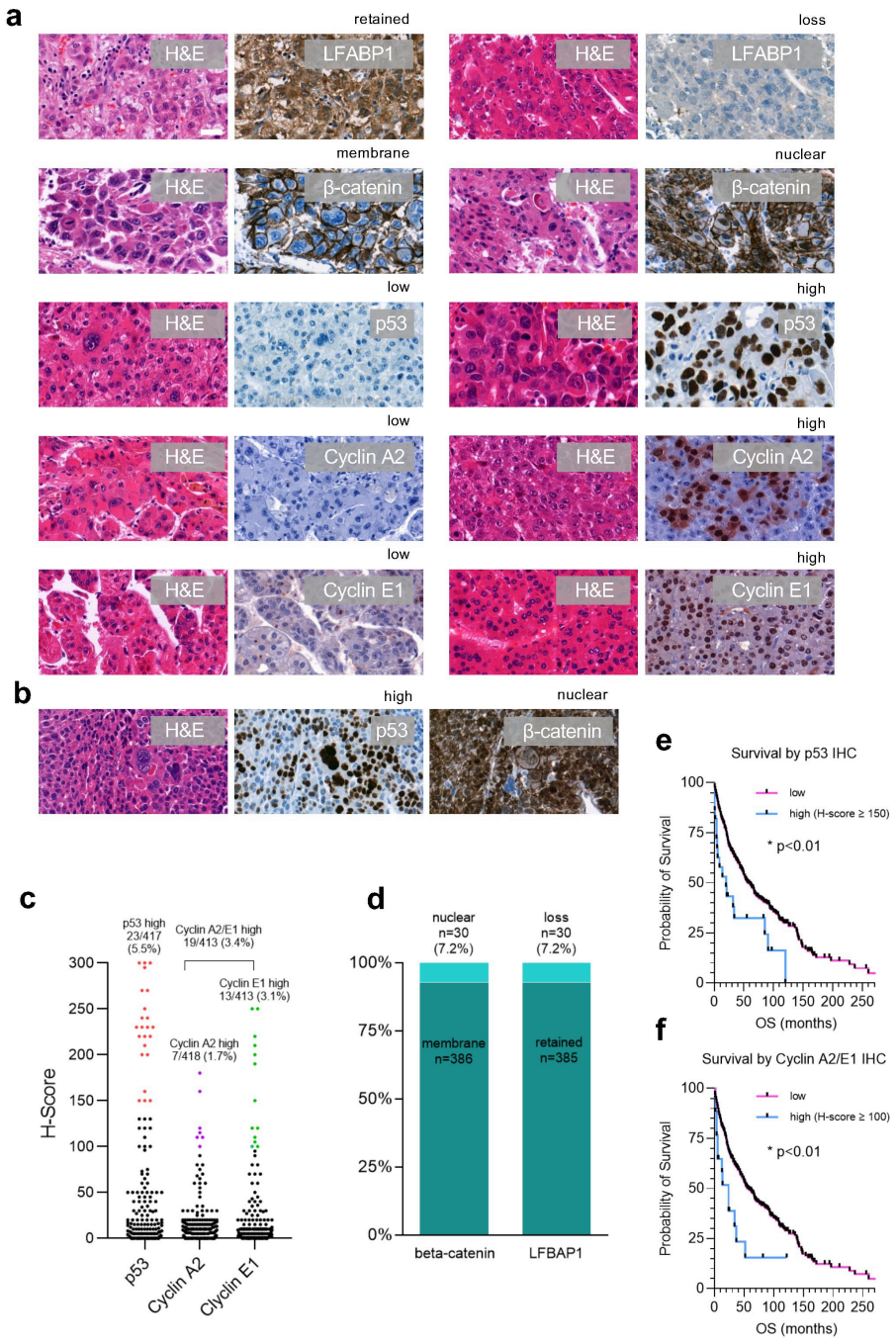


Figure 2

Immunohistochemical characterization and prognostic impact in hepatocellular carcinoma.

(A) Representative hematoxylin and eosin (H&E) sections and corresponding immunohistochemical stainings. The upper row shows L-FABP1 expression with retained cytoplasmic staining in the left panel and loss of expression in the right panel. The second row depicts β-catenin expression, with membranous staining in the left panel (not indicative of mutation) and nuclear accumulation in the right panel, consistent with an underlying mutation. The third row shows p53 expression patterns, with low (wild-type–like) expression in the left panel and high (overexpression) in the right panel. The fourth row illustrates Cyclin A2 expression with representative examples of low (left) and high (right) expression levels. The fifth row shows Cyclin E1 expression, likewise demonstrating low (left) and high (right) expression patterns. Scale bar: 25 μm. **(B)** Exceptional case demonstrating concomitant nuclear overexpression of p53 and nuclear accumulation of β-catenin within the same tumor, suggesting co-occurrence of underlying molecular alterations. **(C)** Quantitative assessment of immunohistochemical expression levels using H-scores for p53, Cyclin A2, and Cyclin E1. Individual cases are displayed as dots, with high-expression subgroups highlighted by color: p53-high cases are indicated in red (defined as H-score ≥150), Cyclin A2–high cases in purple (H-score ≥100), and Cyclin E1–high cases in green (H-score ≥100). Percentages of high-expression cases are provided in brackets; the proportion of cases with combined high expression of Cyclin A2 and/or Cyclin E1 is additionally indicated. **(D)** Distribution of immunohistochemical expression patterns shown as parts-of-a-whole bar graphs. The left panel illustrates β-catenin expression patterns, comparing membranous versus nuclear localization with corresponding percentages. The right panel shows L-FABP1 expression status, comparing retained versus lost expression, with absolute numbers of cases and percentages indicated. **(E)** Overall survival according to p53 immunohistochemical expression status, presented as Kaplan–Meier curves comparing high (H-score ≥150) versus low expression, with median overall survival indicated (time in months); a statistically significant difference is observed ($p < 0.01$). **(F)** Overall survival stratified by combined Cyclin A2/E1 expression status, shown as Kaplan–Meier curves comparing Cyclin A2/E1–high versus Cyclin A2/E1–low subgroups; a statistically significant difference in survival is observed ($p < 0.01$).

Figure 3

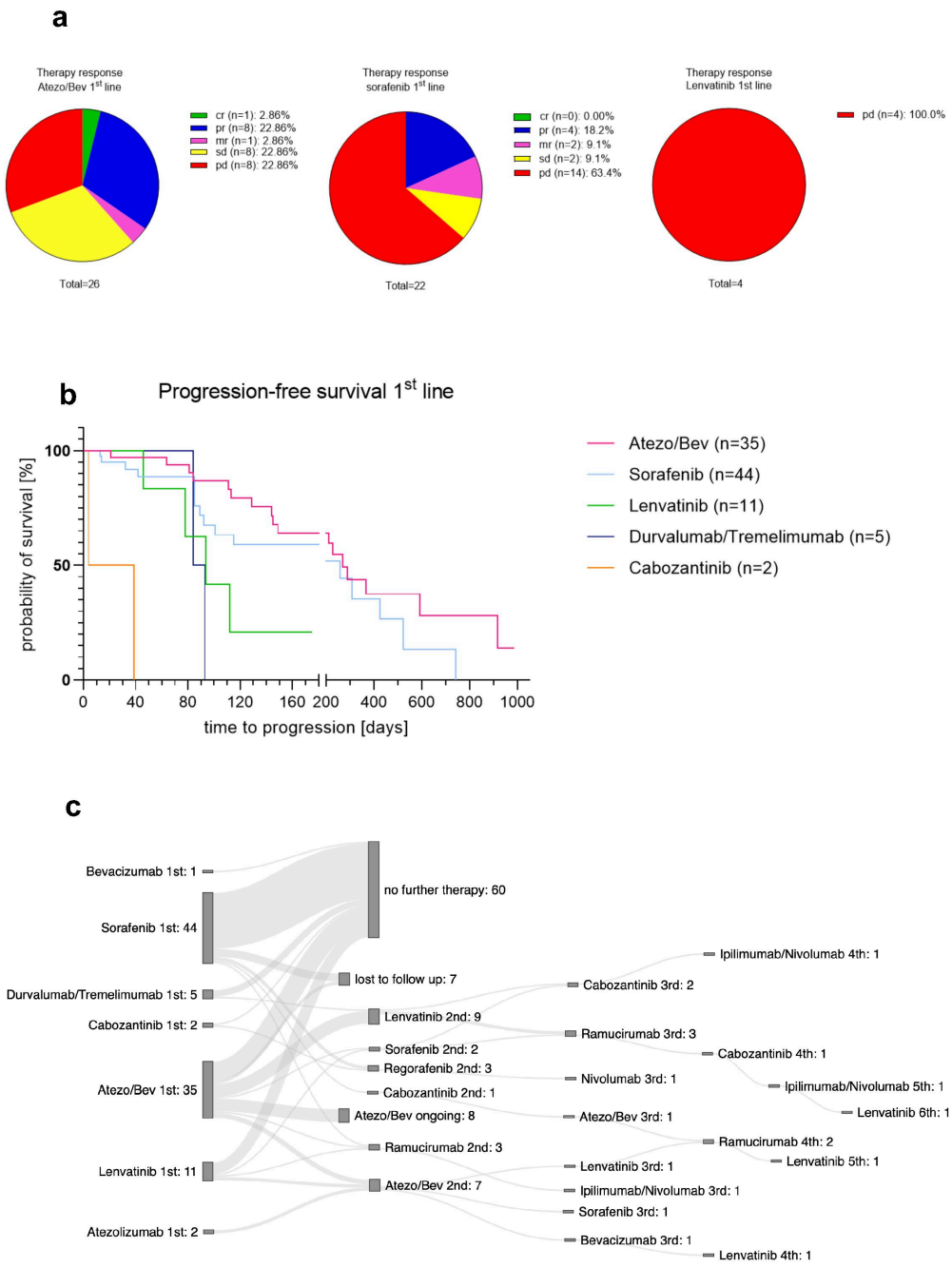


Figure 3

Systemic therapy response patterns and progression-free survival in hepatocellular carcinoma.

(A) Pie charts illustrating best overall response to systemic therapies, categorized as complete response (CR), partial response (PR), mixed response (MR), stable disease (SD), and progressive disease (PD), with corresponding color coding as indicated in the legend. Percentages are shown for each category.

Separate charts are provided for Atezolizumab/Bevacizumab combination therapy, Sorafenib, and Lenvatinib. **(B)** Kaplan–Meier curves of progression-free survival for first line treatment, with time to progression (months) on the x-axis and probability of progression-free survival on the y-axis, stratified by systemic therapy: Atezolizumab/Bevacizumab, Sorafenib, Lenvatinib, DurvalumabTremelimumab, and Cabozantinib, each indicated by distinct colors. **(C)** Alluvial plots (Diagram created using SankeyMATIC) depicting treatment sequences and clinical outcomes. The first column represents the initial systemic therapy administered, while subsequent columns illustrate subsequent lines of therapy or clinical outcomes, visualizing transitions between treatments across the patient cohort.

Supplementary Files

This is a list of supplementary files associated with this preprint. Click to download.

- Supplementarytables.docx
- supplementaryfigures.pdf